Real Freshwater Flux as a Natural Boundary Condition for the Salinity Balance and Thermohaline Circulation Forced by Evaporation and Precipitation

RUI XIN HUANG

Department of Physical Oceanography, Woods Hole Oceanographic Institution, Woods Hole, Massachusetts

(Manuscript received 24 March 1992, in final form 20 January 1993)

ABSTRACT

Freshwater flux used as a natural boundary condition for the salinity balance is applied to a primitive equation model of the oceanic general circulation. Instead of the relaxation condition or the virtual salt flux boundary conditions used in many existing models, the real freshwater flux across the upper surface is specified as the vertical velocity boundary condition for the continuity equation, and the salinity flux is set to identically zero at the sea surface. Numerical experiments show that a model with the natural boundary conditions runs smoothly.

Much important physics involving the freshwater flux emerge from the new model. The barotropic Goldsbrough–Stommel gyres driven by the precipitation and evaporation, which were excluded in the previous numerical models, are reproduced. In addition, the model's results reveal extremely complex structure of the three-dimensional circulation driven by the freshwater flux. In fact, a relatively small amount of freshwater flux drives very strong meridional and zonal cells and baroclinic gyres, which are 100 times stronger than the driving freshwater flux. Most importantly, the model provides an accurate description of the meridional salt fluxes and their roles in setting up the thermohaline circulation. It is suggested that, with or without the rigid-lid approximation, the real freshwater flux can be used as the upper boundary condition in oceanic general circulation models, including the mixed-layer models, the ice–ocean coupling models, and atmosphere–ocean coupling models.

1. Introduction

Oceanic circulation is an essential part of the climate system. Although much progress has been made in simulating the oceanic general circulation, several important issues remain challenging. One of these problems is the improper boundary conditions used for calculating salinity in most existing primitive equation models.

In many numerical models both the temperature and salinity are forced by relaxation conditions at the upper surface. The implementation of the relaxation condition to oceanic general circulation models can be traced back to the early work by Haney (1971). After carefully analyzing the heat flux budget across the air–sea interface, including the incoming solar radiation, back (longwave) radiation, sensible heat, and latent heat, Haney proposed a simple parameterization of the air–sea heat flux:

$$H_f = \Gamma \rho c_p (T^* - T),$$

where Γ is a relaxation coefficient, whose value is about 0.70 m d^{-1}, and T^* is the reference temperature. Both Γ and T^* can be chosen within a certain range. This parameterization for air–sea heat flux has been used extensively in oceanic general circulation studies.

In many existing models the same relaxation condition has been used for the salinity flux. The implementation of a relaxation condition for salinity has very little physical justification. An advantage of the relaxation condition is that models based on this type of condition can reproduce the temperature and salinity distribution that fits observations at the sea surface. The disadvantage of the relaxation condition is the diagnostic nature of the boundary condition—that is, a model based on such a boundary condition can fit the data—however, it gives no dynamic explanation why the surface temperature and salinity pattern exists as observed. This upper boundary condition for the salinity may be tolerable as long as we are just interested in simulating the present-day ocean circulation, whose salinity distribution on the sea surface has been observed for a long time. Recent advances in climate modeling, however, have posed questions about the climate system under conditions different from those of the present day. The surface temperature and salinity under such situations are unknown. In fact, surface temperature and salinity should be calculated as a part of the solution of a complete climate model. Similarly, the application of the relaxation condition to ocean forecasting is questionable.

For a long time numerical modelers were content

Contribution No. 8002 from the Woods Hole Oceanographic Institution.

Corresponding author address: Dr. Rui Xin Huang, Department of Physical Oceanography, Woods Hole Oceanographic Institution, Woods Hole, MA 02543.

with the single stable solution provided by models based on the relaxation condition for temperature and salinity. The possibility of having multiple solutions under the more realistic boundary conditions was largely ignored. The study of multiple solutions for the thermohaline circulation can be traced back to the early work by Stommel (1961). The connection between multiple solutions of the thermohaline circulation with the freshwater flux has been emphasized by Rooth (1982) in his review paper on hydrology and oceanic circulation. Broecker et al. (1985) posed the question of whether the ocean–atmosphere system has more than one stable mode. This question has been answered positively by Bryan (1986), who produced the first pair of multiple solutions in an oceanic general circulation model.

To find the multiple solutions Bryan (1986) designed some special techniques that are still widely used. His approach can be summarized as the following. First, run the model forced by relaxation conditions for both temperature and salinity to a quasi equilibrium. Second, diagnose the equivalent salt flux required for maintaining the salinity balance. Third, run the model with the diagnosed salt flux as the boundary condition for the salinity. Since the relaxation condition still applies to the temperature balance, the boundary conditions in the third step are generally called the mixed boundary conditions.

As Bryan (1986) found, solutions obtained at the first step are generally not very stable to the mixed boundary conditions. Under small perturbations these solutions drift away. Although the so-called mixed boundary conditions have been known for a long time, the instability and drifting phenomenon have been the major difficulties.

A common shortcoming in both the relaxation boundary condition and the mixed boundary conditions is the requirement of an unphysical virtual salt flux through the atmosphere. In the oceans, salinity balance is actually determined by freshwater flux across the air–sea interface, and the salt flux across the air–sea interface is practically zero. The freshwater flux across the air–sea interface is an important component of the ocean–atmosphere coupled system. In the oceans this plain water flux controls the salinity balance, so it is a major player in the thermohaline circulation.

Hough (1897) first considered the saline circulation driven by evaporation and precipitation. Since he did not know how to parameterize friction, his discussion was limited to the spinup phase of the saline circulation. Goldsbrough (1933) obtained a closed saline circulation in the North Atlantic by assuming a very special geographic distribution of evaporation minus precipitation. Stommel (1957, 1984) pointed out that, in principle, circulation driven by evaporation minus precipitation in the ocean interior can be closed by western boundary currents. Recently, the barotropic Goldsbrough–Stommel circulation in the world oceans has been discussed by Huang and Schmitt (1992).

The barotropic Goldsbrough–Stommel circulation has been ignored for long time, partially because it is relatively weak compared with the wind-driven circulation. A simple scaling analysis indicates that the $E - P$ driven barotropic mass fluxes are about 1 Sv or less ($1\ \text{Sv} \equiv 10^6\ \text{m}^3\ \text{s}^{-1}$); this is about a few percent of the wind-driven or the thermally driven circulation). However, a close examination reveals that there is no role for the salinity in their solution. If there was no salinity difference between the rainwater and seawater, the Goldsbrough–Stommel gyres would be a perfect description for the $E - P$ driven circulation. However, the $E - P$ induced dilution/concentration of salt gives rise to a very strong and complicated baroclinic structure of the saline circulation.

The salt mixing–induced recirculation in salty estuaries is well known. Freshwater input F from river runoff is relatively small. If there were no mixing, the only motion would be confined to a thin layer of plain water on the top, Fig. 1a. However, there is mixing induced by tide, waves, or wind stress, so salt is entrained into the upper layer, Fig. 1b. Assuming a steady state, the salt balance gives

$$(F + R)S_0 = RS_b; \tag{1}$$

thus, the return flow is

$$R = \frac{S_0}{S_b - S_0} F. \tag{2}$$

Generally, $S_0 \approx S_b$ due to strong mixing, so $R \gg F$; that is, the return flow is many times larger than the river runoff.

Similarly, the North Atlantic can be treated as a huge estuary. Assume precipitation at high latitudes is ex-

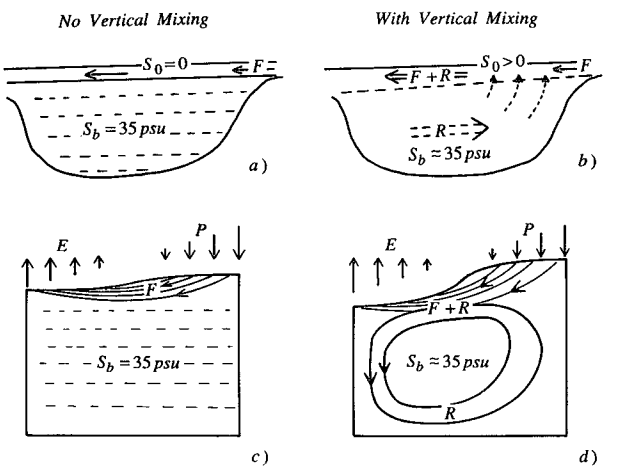

FIG. 1. Schematic models of plain water–driven circulation. (a) and (b) River runoff (F)-driven circulation in a salty estuary; (c) and (d) evaporation minus precipitation-driven circulation in a closed basin. The vertical scales are exaggerated, especially the free surface elevations.

actly balanced by precipitation at low latitudes (Fig. 1c and 1d). First, let us assume there is absolutely no mixing. At time $t = 0$, rainwater starts to come into the subpolar basin and evaporation starts at low latitudes. Precipitation at high latitudes builds up the free surface, and water starts to flow toward low latitudes (rotation modifies the path). At low latitudes in the beginning evaporation would make some water saltier, which sinks to depth; this would give rise to motion in the salty water. However, as fresh water arrives in low latitudes and gradually covers the entire upper surface of the basin, evaporation can affect only the fresh water, but not the salty water. As the residual motions in the deep water gradually lose their kinetic energy, the only motion will be the equatorward flow of fresh water on top of stagnant deep, salty water (Fig. 1c).

Second, if there is vertical mixing, there will be a very strong return flow induced by vertical mixing:

$$R = \frac{S_0}{\Delta S} F \gg F.$$

Because ΔS is much less than S_0, a small amount of precipitation can drive a strong meridional circulation. Because of the horizontal pressure gradient due to the stratification, the meridional gradient of free surface elevation in the case with mixing is much larger than the case without mixing.

Although it is believed that the freshwater forcing is as important as the thermal forcing in determining the thermohaline circulation, the fresh water–forced circulation has been basically ignored. In fact, fresh water–forced large-scale circulation is not mentioned in most textbooks on oceanic circulation. Because most existing oceanic general circulation models assume vertical velocity to be exactly zero at the sea surface, the Goldsbrough–Stommel gyres are excluded from these models. Thus, the water cycle through the atmosphere and the oceans is not simulated correctly. It is time to examine the dynamical roles of freshwater flux. As the first step, it seems interesting and important to study the simplest possible case—a saline circulation forced by freshwater flux alone.

The outline of this paper is the following. First, different boundary conditions for the salinity balance will be analyzed. In particular, the disadvantages and pitfalls of the virtual salt flux condition will be emphasized. Second, the freshwater flux condition under the so-called rigid-lid approximation will be applied to the Bryan–Cox model. Third, the model will be used to study a saline circulation forced by freshwater flux alone. In fact, the focus of this study is to examine the three-dimensional structure of the saline circulation. In addition, the differences between the new model and the old models will be examined.

2. Three types of boundary conditions for the salinity balance

In this section the focus is on different types of boundary conditions for the saline circulation in the x–z plane. For convenience, Cartesian coordinates will be used in this section.

The salinity balance in a surface box, shown in Fig. 2, can be written as

$$\frac{\partial S}{\partial t} + \frac{1}{\Delta x}[(uS)^+ - (uS)^-] + \frac{1}{\Delta z}[(wS)^+ - (wS)^-] = \frac{A_s}{\Delta x}(S_x^+ - S_x^-) + \frac{k_s}{\Delta z}(S_z^+ - S_z^-), \quad (3)$$

where $(uS)^+$ and $(uS)^-$ are the salt flux advected across the right and left boundaries, S_x^+ and S_x^- are the horizontal salinity gradient at the right and left boundaries; similarly, $(wS)^+$ and $(wS)^-$ are the salt flux advected through the upper and lower boundaries, and S_z^+ and S_z^- are the vertical salinity gradient at the upper and lower boundary; A_s and k_s are the horizontal and vertical diffusivity for the salt, and $S_f = k_s S_z^+$ is the turbulent salt flux cross the air–sea interface. In addition, vertical velocity is prescribed on the upper surface:

$$w = w^+, \quad \text{at} \quad z = 0. \quad (4)$$

a. Relaxation condition

(i) $w^+ = 0$: so $(wS)^+$ vanishes. This boundary condition is usually called the rigid-lid condition. As will be discussed shortly, the rigid-lid approximation does not necessarily require the vertical velocity to be zero at the upper surface.

(ii) $S_f = \Gamma(S^* - S)$: where S^* is specified according to climatological mean surface salinity.

b. Mixed boundary condition

(i) $w^+ = 0$: so $(wS)^+$ vanishes.

(ii) $S_f = (E - P)S$: where E and P are the evaporation and precipitation, and S is the salinity in the box. This is the virtual salt flux required for the salinity balance.

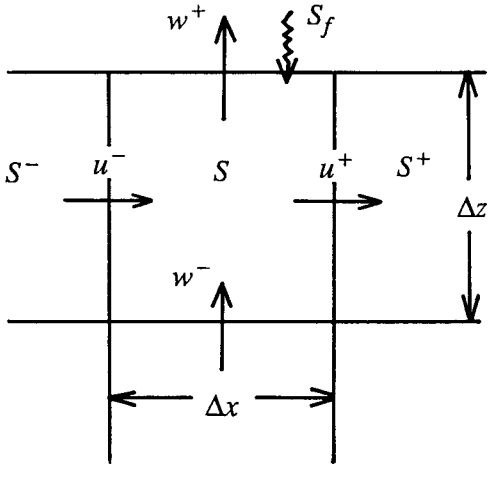

FIG. 2. A finite-difference grid box in the x–z plane.

c. Natural boundary condition

(i) $w^+ = E - P$: this is the freshwater flux controlling the salinity balance.

(ii) $(wS)^+ - k_s S_z^+ = 0$: Note that within the water column there is always a turbulent salt flux $k_s S_z$ and an advective salt flux wS. However, in the air there is no salt, so both these terms are identically zero, although w is not zero. At the air–sea interface the turbulent flux must exactly cancel the advective flux so that there is absolutely no salt flux across the air–sea interface, as required by the physics. Thus, we may call this turbulent flux $S_f = k_v S_z$ an antiadvective salt flux. As seen from the preceding discussion, $S_f = (E - P)S$ below the air–sea interface; however, this flux is identically zero above the water because there is no salt advection and no need for the antiadvective salt flux.

Accordingly, the salinity balance for a surface box is reduced to

$$\frac{\partial S}{\partial t} + \frac{1}{\Delta x}[(uS)^+ - (uS)^-] - \frac{1}{\Delta z}(wS)^- = \frac{A_s}{\Delta x}(S_x^+ - S_x^-) - \frac{k_s}{\Delta z} S_z^-. \quad (3')$$

If the mixing terms are negligible, the total salt is conserved, so the local salinity change is due to freshwater dilution/concentration.

In many previous mixed-layer models and primitive equation models for the oceanic general circulation the so-called "rigid-lid" approximation has been interpreted as equivalent to setting the vertical velocity to zero at the sea surface. Without a vertical flux of plain water through the upper surface, the salinity change due to evaporation and precipitation has to be simulated by the virtual salt flux as discussed. Therefore, the so-called antiadvective salt flux has been substituted as a forcing to simulate the salt balance. However, the essential assumption of the rigid-lid approximation is to move the upper boundary from the free surface $z = \eta$ to the rigid lid $z = 0$, and it is not inconsistent with adding a small vertical velocity at the air–sea interface. As long as we are only concerned about large-scale geostrophic motions of climate time scales, the rigid-lid approximation is valid (see the Appendix).

In fact, the rigid-lid approximation has been used in many models with nonzero vertical velocity at $z = 0$. For example, in many quasigeostrophic models the dynamic effect of wind stress curl is simulated by imposing the equivalent Ekman pumping velocity at the upper surface. In general, the Ekman pumping velocity is about 30 times larger than the vertical velocity associated with precipitation and evaporation. Since all these quasigeostrophic numerical models have been used extensively without any trouble associated with the nonzero vertical velocity on the upper surface, this should be true for the primitive equation models too. For motions of planetary scale or motions associated with seasonal time scale (or shorter), the rigid-lid assumption may not be valid, and a free surface should be included in the calculation.

d. The pitfalls of the relaxation and mixed conditions

These three boundary conditions are quite different in their physical meaning and numerical stability. Since the relaxation condition is a negative feedback, the solutions are stable. Notice that the oceanic circulation is a turbulent system, so it is essentially a chaotic system. When we say the solution obtained using the relaxation condition is stable, we only mean that there is no instability directly associated with the boundary condition.

Although the ability to match the observed surface salinity may be an advantage for simulating the present climate, it may not be suitable for simulating the oceanic circulation for general situations. For example, the surface salinity for the world oceans in the remote past and in the future is unknown, so the relaxation condition cannot apply. The implementation of the relaxation condition also eliminates the possibility of getting into some other possible modes of the thermohaline circulation. Similarly, using the salinity relaxation condition for oceanic forecasting is questionable because neither the reference salinity distribution S^* nor the suitable relaxation constant is clear.

The natural condition is a zero salt flux condition, so its numerical stability may be similar to that of the mixed conditions. However, these two boundary conditions are different in terms of physics and numerical implementation. To illustrate the essential difference between the virtual salt flux condition and the natural condition, let us consider the following simple cases. Assume that the size of the grid box is of one unit and there is neither horizontal nor vertical diffusion; that is, A_s and k_s are zero. In addition, $w = 0$ at the lower interface. An upwind scheme is used for the finite difference.

Based on the natural boundary condition, the salinity balance and continuity equations give

$$\frac{DS}{Dt} = \frac{\partial S}{\partial t} + u^+ S - u^- S^- = 0, \quad (5)$$

$$u^+ = u^- + P - E. \quad (6)$$

Suppose $P - E = 0$ and $S^- = S$ at initial time $t = 0$. For $t > 0$, fresh water (precipitation) enters from above, $P - E > 0$. Within a short time period after the freshwater flux is turned on, the salinity is practically uniform—$S^- \approx S$—so the local salinity changes according to

$$\frac{\partial S}{\partial t} \approx -(P - E)S. \quad (7)$$

The salinity decreases due to freshwater dilution; there

is no need for virtual salt flux. Notice that this is the essential difference between the present boundary condition and the relaxation boundary condition and the mixed boundary conditions where the virtual salt flux is essential for the salinity balance in the surface boxes.

For long time, the salinity approaches

$$S = \frac{u^-}{u^- + P - E} S^- \approx \left(1 - \frac{P - E}{u^-}\right) S^-. \quad (8)$$

Therefore, freshwater flux gives rise to the horizontal salinity gradient generated by dilution/concentration, which drives the oceanic circulation.

In comparison, the salt balance for the case of mixed boundary conditions gives

$$\frac{DS}{Dt} = \frac{\partial S}{\partial t} + u(S - S^-) = -(P - E)S, \quad (9)$$

where $u^+ = u^- = u$ is forced by the continuity equation. As $t \to \infty$, the salinity approaches

$$S = \frac{u}{u + P - E} S^- \approx \left(1 - \frac{P - E}{u}\right) S^-. \quad (10)$$

Although these two models look the same, they have totally different physical meaning and their numerical instability could be quite different.

There are essential difficulties associated with the first and second types of boundary conditions. First, to balance the salt in the oceans a huge virtual salt flux through the air–sea interface and the atmosphere is required for taking up the salt from the subpolar basin, transporting it equatorward, and depositing it there (Fig. 3a). The virtual salt flux required in the North Atlantic can be estimated as

$$\sum (E - P)S \approx 0.3 \times 10^9 \text{ kg s}^{-1} \times \frac{35}{1000} \approx 1.05 \times 10^7 \text{ kg s}^{-1}. \quad (11)$$

It is worth noting that such a virtual salt flux must continue to flow poleward in the ocean; thus, this virtual salt flux would appear as the meridional salt flux across zonal sections based on these old models. In reality, there is a water cycle going through the atmosphere–ocean coupled system, and the virtual salt flux is a misinterpolation of the water cycle (Fig. 3b). Since the hydrologic cycle is an important part of the ocean–atmosphere coupled system, it is much better to simulate the water cycle directly and avoid any confusion associated with the virtual salt flux.

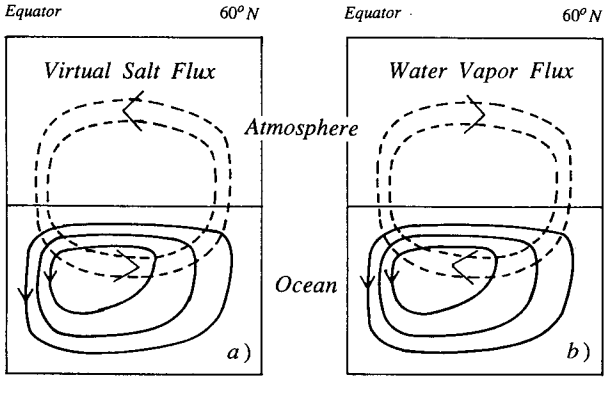

FIG. 3. (a) Meridional circulations in an atmosphere–ocean coupled model. Old models based on virtual salt flux. (b) New model based on natural boundary condition of plain water flux.

Second, the original definition of virtual salt flux includes a positive (negative) feedback wherever evaporation is stronger (weaker) than precipitation. Such a feedback is unphysical, although it is rather weak. In addition, using the $(E - P)S$ to force a model can cause the total salt in a basin to increase unboundedly. The argument is very simple indeed. At the present day, the global integration of precipitation minus evaporation should be zero:

$$\iint (E - P)dA = 0, \quad (12)$$

where water storage on land is ignored. However, the global integration of the virtual salt flux is larger than zero:

$$\iint (E - P)SdA > 0. \quad (13)$$

This is due to a positive correlation between evaporation and high salinity. For example, evaporation is very strong in the subtropical North Atlantic, which gives rise to a salinity of more than 37 psu; meanwhile, excess precipitation in the subpolar Pacific gives rise to a surface salinity lower than 33 psu. Thus, to avoid the salinity explosion one must use the virtual salt flux defined by

$$S_f = (E - P)\bar{S}_s, \quad (14)$$

where $\bar{S}_s$ is the mean sea surface salinity averaged over the whole domain of the model. The new form (14) eliminates the unwanted feedback between local salinity and salt flux and the global salinity explosion. However, this constraint can introduce large errors wherever the local salinity is much different from the basin or global mean. For example, surface salinity in the North Pacific can be lower than 33 psu, and the surface salinity in the North Atlantic can be higher than 37 psu. Suppose $\bar{S}_s$ is defined as 35 psu for a World Ocean circulation mode; a systematic bias of 10% will be introduced through the upper boundary condition for the salinity.

The errors introduced by replacing S with $\bar{S}_s$ can be very large near the river mouths or ice edge, especially for high-resolution models. For example, salinity can be lower than 10 psu near the mouth of the Amazon River. A model based on the virtual salt flux would

impose a salt flux several times larger than it should be. As a result, the local salinity could become negative (Syukuro Manabe 1992, personal communication).

The other difficulty associated with the virtual salt flux formulation is that the salt flux depends on the mean sea surface salinity, which is unknown before the whole solution is determined. In fact, $\bar{S}_s$ can change as the solution evolves and the time evolution of $\bar{S}_s$ itself gives rise to some uncertainty of the salt flux. For example, in numerical experiments involving halocline catastrophe in a single-hemisphere basin, a model is first spun up to a quasi equilibrium under the relaxation condition for the salinity. Then, the equivalent salt flux is diagnosed and used as a flux condition for the second stage of the experiment where the halocline catastrophe takes place. The mean sea surface salinity is relatively high (for example, 36.5 psu) during the first stage because the system is in a thermal mode; however, the mean sea surface salinity is relatively low (for example, 33.5 psu) after the halocline catastrophe because the system is in a saline mode. If the virtual salt flux was defined using the instantaneous mean surface salinity, it should have been reduced by 10% during the transition from the thermal mode to the saline mode. However, in previous numerical experiments, the virtual salt flux is fixed throughout the entire numerical experiment. In some sense, the salt flux used in the final stage of these experiments is exaggerated about 10%. There has been much evidence suggesting that the behavior of the system is very sensitive to the flux imposed, so it seems important to reexamine these numerical experiments with a model based on the natural boundary condition.

Although the virtual salt flux has been used in general circulation models only within the past few years, it has been used in many books and papers involving air–sea interaction for a long time. For example, a virtual salt flux, $(P_0 - E_0)S_0$, appeared in the salinity equation in the classic paper by Niiler and Kraus (1977). As discussed here, this virtual salt flux is nonphysical. In addition, the global salinity conservation requires replacement of the local S_0 with the global mean $\bar{S}_s$; thus errors are introduced through use of the virtual salt flux.

The natural boundary conditions for the salinity balance have been used in a study of the multiple equilibrium states of the thermohaline circulation based on simple box models by Huang et al. (1992). In this study the focus will be on a general circulation model without a mixed layer; however, the same principles apply to all other cases involving freshwater flux across the air–sea interface, including mixed-layer models, ice–ocean coupling models, and atmosphere–ocean coupling models.

Similarly, the current way of treating the river runoff as distributed evaporation minus precipitation over some latitude band is inaccurate. The suitable way is to treat the fresh water from river runoff as just plain water (with zero salinity) entering the ocean by specifying the horizontal velocity normal to the coast.

3. The numerical model

In this section a numerical model is formulated using the freshwater flux at the sea surface as the natural boundary condition for the salinity balance. The notation will follow that of Bryan (1969a), and the discussion is limited to the part that is different from Bryan's original model. The reader is referred to the original paper by Bryan for some numerical detail.

In spherical coordinates it is convenient to define an advection operator

$$L\mu = \frac{m}{a}[(u\mu)_\lambda + (v\mu/m)_\phi)] + (w\mu)_z, \quad (15)$$

where μ is some scalar quantity, a is the radius of the earth, ϕ is latitude, λ is longitude, and

$$m = \sec\phi, \quad (16)$$

$$n = \sin\phi, \quad (17)$$

$$u = a\dot{\lambda}/m, \quad (18)$$

$$v = a\dot{\phi}. \quad (19)$$

The equations of motion may be written as

$$u_t + Lu - 2\Omega nv - mnuv/a = -\frac{m}{a}(p/\rho_0)_\lambda + F^\lambda \quad (20)$$

$$v_t + Lv + 2\Omega nu + mnuu/a = -\frac{1}{a}(p/\rho_0)_\phi + F^\phi. \quad (21)$$

The hydrostatic relation is

$$\rho g = -p_z, \quad (22)$$

and the continuity equation is

$$w_z + \frac{m}{a}[u_\lambda + (v/m)_\phi] = 0. \quad (23)$$

The temperature and salinity satisfy conservation equations

$$T_t + LT = Q, \quad (24)$$

$$S_t + LS = \sigma. \quad (25)$$

The terms F^λ, F^ϕ, Q, and σ represent the turbulent viscosity and mixing.

The upper boundary conditions for the velocity are

$$\rho_0 k_m(u_z, v_z) = \tau^\lambda, \tau^\phi \quad \text{at} \quad z = 0, \quad (26)$$

$$w_0 = E - P \quad \text{at} \quad z = 0, \quad (27)$$

where k_m is the vertical momentum diffusivity, E is the evaporation rate, and P is the precipitation rate, in

centimeters per second. The upper boundary conditions for the temperature and salinity in terms of flux are

$$T_f = \Gamma(T^* - T), \tag{28}$$

$$wS - k_s S_z = 0. \tag{29}$$

Notice that a relaxation condition is applied to the temperature, although other types of boundary conditions can be applied to the temperature calculation as well. The major difference from the traditional models is the boundary condition for the salinity.

At the lower boundary the corresponding boundary conditions are

$$\rho_0 k_m(u_z, v_z) = \tau_B^\lambda, \tau_B^\phi \tag{30}$$

$$w(-H) = -\frac{u(-H)}{a} mH_\lambda - \frac{v(-H)}{a} H_\phi \tag{31}$$

$$T_z = S_z = 0, \quad \text{at} \quad z = -H. \tag{32}$$

The lateral boundary conditions are the same as described by Bryan (1969a).

a. How to calculate the barotropic velocity

The horizontal velocity field is decomposed into two parts, a barotropic component and a baroclinic component. The barotropic velocity can be calculated by using a depth-integrated version of the horizontal momentum equations [(20), (21)]. However, the pressure terms on the right-hand side are still unknown. There are basically two ways to overcome this difficulty. First, one can use a vertically integrated continuity equation to predict the free surface elevation. As long as the free surface elevation is known, the pressure term can be calculated using the hydrostatic approximation. Due to advances in altimetry data there has been some effort to develop models with a free surface; for example, see Killworth et al. (1991). Second, the pressure term can be eliminated by introducing a barotropic streamfunction. Thus, instead of using very small time steps or some implicit scheme to calculate the free surface, the problem is reduced to solving an elliptic equation at each time step. Since an elliptical equation can be solved by iteration, for the cases of low resolution and simple geometry this approach can save computing time compared with the first approach, and this is what has been used in the Bryan–Cox model.

In the present model a similar approach is used. First, integrating the continuity equation (23) and using boundary conditions (26), (31) gives

$$\left(\int_{-H}^{0} u dz\right)_\lambda + \left(\int_{-H}^{0} \frac{v}{m} dz\right)_\phi = -\frac{a}{m}(E - P). \tag{33}$$

Now the depth-integrated velocity is not divergence free. It is well known that any velocity field can be described in terms of a streamfunction plus a potential function. Paralleling Bryan (1969a), a barotropic streamfunction Ψ and a barotropic potential function Φ is introduced:

$$a\int_H^0 \rho_0 u dz = -\Psi_\phi + m\Phi_\lambda, \tag{34}$$

$$a\int_{-H}^{0} \rho_0 v dz = m\Psi_\lambda + \Phi_\phi. \tag{35}$$

Cross-differentiating and adding (34), (35) gives

$$\frac{m^2}{a^2}\Phi_{\lambda\lambda} + \frac{m}{a^2}\left(\frac{1}{m}\Phi_\phi\right)_\phi = -\rho_0(E - P). \tag{36}$$

This equation should be solved with the no-flux boundary condition along the edge of the basin; that is, $\partial\Phi/\partial n = 0$ along the lateral boundary. If $E - P$ is independent of time, Eq. (36) needs to be solved only once. However, if $E - P$ is allowed to vary with time, this equation has to be solved for each time step.

Introducing the surface pressure p_s, one can write the pressure as

$$p(z) = p_s + g\int_z^0 \rho dz. \tag{37}$$

Notice that p_s is the unknown pressure required for the rigid-lid approximation.

The time evolution of the barotropic streamfunction can be obtained by integrating the momentum equations (20), (21) over the depth of the ocean and multiplying by $a\rho_0/mH$ and $a\rho_0/H$, respectively:

$$-\left(\frac{\Psi_\phi}{Hm}\right)_t + \left(\frac{\Phi_\lambda}{H}\right)_t = -(p_s)_\lambda + \frac{2\Omega n}{H}\left(\Psi_\lambda + \frac{1}{m}\Phi_\phi\right) + \frac{FU}{m}, \tag{38}$$

$$\left(\frac{m\Psi_\lambda}{H}\right)_t + \left(\frac{\Phi_\phi}{H}\right)_t = -(p_s)_\phi + \frac{2\Omega n}{H}(\Psi_\phi - m\Phi_\lambda) + FV, \tag{39}$$

where

$$FU = \frac{-a\rho_0}{H}\int_{-H}^{0}\left(Lu - mnuv/a - F^\lambda + \frac{gm}{a\rho_0}\int_z^0 \rho_\lambda dz'\right)dz, \tag{40}$$

$$FV = \frac{-a\rho_0}{H}\int_{-H}^{0}\left(Lv + mmuu/a - F^\phi + \frac{g}{a\rho_0}\int_z^0 \rho_\phi dz'\right)dz. \tag{41}$$

The surface pressure term can be eliminated by cross- differentiating and subtracting (38), (39)

$$\left(\frac{m\Psi_\lambda}{H}\right)_{\lambda t} + \left(\frac{\Psi_\phi}{Hm}\right)_{\phi t} = \left(\frac{\Phi_\lambda}{H}\right)_{\phi t} - \left(\frac{\Phi_\phi}{H}\right)_{\lambda t} + (FV)_\lambda - (FU/m)_\phi$$
$$- \left(\Psi_\lambda + \frac{1}{m}\Phi_\phi\right)\left(\frac{2\Omega n}{H}\right)_\phi + (\Psi_\phi - m\Phi_\lambda)\left(\frac{2\Omega n}{H}\right)_\lambda + \frac{2\Omega n}{H}\frac{a^2\rho_0}{m}(E-P). \quad (42)$$

This equation is subject to a boundary condition of Ψ = const along the lateral boundary. In this equation Φ is given from previous calculation. Therefore, the computation of the barotropic streamfunction is very similar to the original Bryan–Cox model except for some small additional terms.

Before proceeding with other topics, it is important to understand the meaning of (42). Let us assume a simple case that satisfies the following constraints:

1) $\partial/\partial t \equiv 0$
2) $H \equiv$ const
3) Nonlinear terms, such as Lu, Lv, and uv, are negligible
4) $\rho \equiv$ const
5) $\int_{-H}^{0} F^\lambda dz = \tau_s^\lambda$, $\int_{-H}^{0} F^\phi dz = \tau_s^\phi = 0$
6) Bottom stress is negligible.

Under these assumptions equation (42) is reduced to

$$0 = (a\rho_0\tau^\lambda/m)_\phi - \left(\Psi_\lambda + \frac{1}{m}\Phi_\phi\right)2\Omega\cos\phi + 2\Omega\sin\phi a^2\cos\phi\rho_0(E-P). \quad (43)$$

This can be further reduced to

$$\beta V = f(E-P) - m\left(\frac{\tau^\lambda}{m}\right)_\phi. \quad (44)$$

This is the Goldsbrough–Sverdrup relation for the case with both freshwater flux forcing and wind stress forcing. In the ocean interior the meridional velocity is the superposition of Goldsbrough gyres driven by the evaporation and precipitation:

$$f(E-P)$$

and Sverdrup gyres driven by the wind stress curl:

$$-\left(\frac{\tau^\lambda}{m}\right)_\phi.$$

To close these interior gyres there are western boundary layers that transport water meridionally. Within these boundary currents higher-order terms, such as lateral or bottom friction, dominate.

As discussed, the horizontal velocity is decomposed into two parts:

$$(u, v) = (\bar{u}, \bar{v}) + (\hat{u}, \hat{v}), \quad (45)$$

where $(\bar{u}, \bar{v})$ are the barotropic velocity and $(\hat{u}, \hat{v})$ are the baroclinic velocity. We have discussed how to calculate the barotropic potential function and the barotropic streamfunction. By differentiating these two functions the vertically integrated barotropic velocity $H\bar{u}$ and $H\bar{v}$ are obtained. The calculation of the baroclinic velocity is the same as in the original Bryan–Cox model.

b. Simple cases when Φ is in analytical form

Consider a simple basin confined by two latitude circles and two longitude circles. In addition, assume that the precipitation and evaporation depend on the latitude only; that is,

$$E - P = w_0(\phi). \quad (46)$$

Along the eastern and western boundaries, the no-flow condition requires

$$U_\Phi = \Phi_\lambda = 0 \quad \text{at} \quad \lambda = \lambda_e \quad \text{and} \quad \lambda = \lambda_w. \quad (47)$$

Due to the symmetry of the problem, $U_\Phi = \Phi_\lambda = 0$ is held everywhere. The Poisson equation is reduced to an ordinary differential equation in ϕ, whose first integration is

$$\Phi_\phi = \rho_0 a^2 m \int_\phi^{\phi_n} \frac{w_0}{m}\, d\phi, \quad (48)$$

where ϕ_n is the latitude of the northern boundary. Therefore, the depth-integrated barotropic velocity due to the source is

$$V_\Phi = \frac{a}{\cos\phi}\int_\phi^{\phi_n} w_0\cos\phi d\phi. \quad (49)$$

A consistent constraint must be imposed on the evaporation and precipitation patterns; namely, the basin-integrated freshwater flux must be balanced:

$$\int\int w_0\cos\phi d\lambda d\phi = R, \quad (50)$$

where R indicates the sum of the river runoff along the edge of the basin. If we treat the river runoff as part of precipitation, then the basin integration of w_0 must be exactly zero.

A simple, "linear" profile can be chosen for a basin confined between the equator $\phi = 0$ and the northern

boundary $\phi = \phi_n$ as

$$w_0 = \frac{W_0}{\cos\phi}\left(1 - \frac{2\phi}{\phi_n}\right), \tag{51}$$

where $W_0 > 0$ is the amplitude of precipitation. The corresponding depth-integrated barotropic velocity due to the potential function is

$$V_\Phi = -\frac{aW_0}{\cos\phi}\phi\left(1 - \frac{\phi}{\phi_n}\right). \tag{52}$$

Notice that V is negative everywhere, and it reaches local minimum at $\phi = \phi_n/2$, where

$$V_{\Phi,\min} = -\frac{a\phi_n}{2\cos(\phi_n/2)} W_0 < 0. \tag{53}$$

Since our understanding of the saline circulation is rather elementary, it seems better to use a simple linear profile, so that the structure of the solution is free of dynamical details specific for individual profiles, such as the $E - P$ profiles in the oceans by Baumgartner and Reichel (1985) or Schmitt et al. (1989).

Assume there is no wind stress; the depth-integrated meridional velocity driven by this linearly distributed $E - P$ is

$$V = V_\Phi + V_\Psi = \frac{aW_0 \sin\phi}{\cos^2\phi}\left(1 - \frac{2\phi}{\phi_n}\right). \tag{54}$$

Accordingly, the depth-integrated meridional velocity due to the streamfunction is

$$V_\Psi = \frac{aW_0}{\cos\phi}\left[\frac{\sin\phi}{\cos\phi}\left(1 - \frac{2\phi}{\phi_n}\right) + \phi\left(1 - \frac{\phi}{\phi_n}\right)\right]. \tag{55}$$

Assume a 60° × 60° basin and W_0 = 1 m yr^{-1} $\approx 3 \times 10^{-6}$ cm s^{-1}; the $E - P$ distribution mass fluxes are shown in Fig. 4. The maximum precipitation rate is 0.567×10^{-5} cm s^{-1} at the middle of the northernmost grid box. The slight nonlinearity in the profile is due to the spheric weight function $1/\cos\phi$. The total southward mass flux due to the precipitation minus evaporation reaches a maximum of 0.362 Sv at 30°N.

The interior flow is dictated by the Goldsbrough–Sverdrup relation, and at high latitudes, the mass flux in the ocean interior becomes larger and larger because f/β approaches infinity near the pole. At the same time, the mass flux of the western boundary current required for closing the circulation also increases quickly. Although the barotropic mass flux of the Goldsbrough–Stommel gyres is very small at low latitudes, it is fairly large at high latitudes, and it may be a substantial part of the total barotropic mass flux in the subpolar basin and should not be neglected.

Notice that the velocity component represented by the streamfunction is divergence free, so the meridional mass flux due to the streamfunction in the ocean interior is exactly balanced by an opposite flow within the western boundary currents. Solving (55) for $V_\Psi = 0$ gives $\phi_0 \approx 38.9$°N as the latitude separating the northward western boundary from the southward western boundary current.

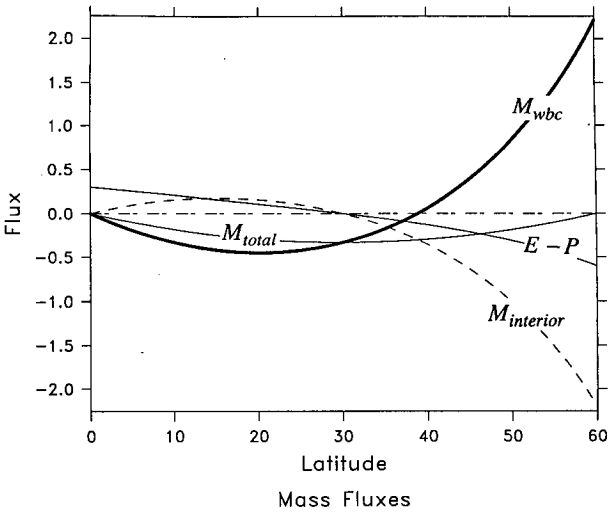

FIG. 4. Meridional distribution of mass fluxes: $E - P$ is the evaporation minus precipitation (in 10^{-5} cm s^{-1}), M_{interior} is the poleward mass flux in the interior, M_{wbc} is the mass flux of the western boundary current, M_{total} is the total poleward mass flux; all these mass fluxes are in Sverdrups.

4. Saline circulation driven by freshwater flux

In this section a simple case will be discussed in which the only forcing is evaporation and precipitation. The basin is confined between the equator and 60°N, and extended 60° zonally. To save computation time, a 4° × 4° low-resolution B-grid model is used in the numerical experiments. The horizontal viscosity (for the velocity) is $A_m = 1 \times 10^9$ cm^2 s^{-1}, and the horizontal diffusivity (for the salinity) is $A_s = 1 \times 10^7$ cm^2 s^{-1}. The vertical viscosity and diffusivity are $k_m = k_s = 1$ cm^2 s^{-1}. The time steps used are dtts = 60 h for the salinity and dtuv = 3 h for the velocity. There are 15 levels vertically, whose depths are 30, 76.3, 143.8, 238.3, 366.8, 537.3, 759.2, 1042.7, 1398.9, 1839.5, 2376.3, 3020.8, 3783.8, 4674.5, and 5700 m.

For the amount of vertical diffusion and vertical resolution, it is clear that the Peclet number may well exceed 2, especially for the deep levels. Although increasing the vertical diffusivity may help to reduce the Peclet number, it also has some side effects. First, large diffusivity is not consistent with oceanic observations. Second, large diffusivity may wipe out some interesting phenomena intrinsic to the system. Third, large diffusivity would induce a large velocity because the circulation is driven by mixing, so increasing the vertical diffusivity may not help much to reduce the Peclet number. Thus, the same values used in many other numerical experiments have been used in this study.

The convective adjustment scheme used in a model may also be very important. It was previously noticed that going through the convective adjustment loop in the standard Geophysical Fluid Dynamics Laboratory code only once for each time step (by default) does not guarantee a complete convective adjustment, and the stratification is not quite stable; for example, see Killworth (1989). In the numerical experiments the convective adjustment loop is repeated five times for each time step to assume a more complete vertical mixing for the unstable columns. It was found that, in the numerical experiments when the convective adjustment loop is used only once per time step, some false finestructure may appear; however, when several cycles of convective adjustment are implemented, the solution becomes smoother.

The simple profile discussed in the previous section is used, with $W_0 = 1$ m yr^{-1} (Fig. 4). The model is spun up from an initially homogeneous state of rest with a uniform salinity equal to 35 psu and temperature equal to 12.5°C. (Notice that temperature will remain constant everywhere because there is no heating or cooling.) After 200 years of calculation, the model enters into a quasi-periodic oscillation. After about 1600 years, the oscillation becomes very regular, although the mean surface salinity still declines slowly. After 1712 years, the model reaches a state characterized by an oscillation period of 18.87 years (Fig. 5). During the spinup process the mean sea surface salinity declines continuously and eventually settles to about 33.76 psu with an oscillation amplitude of 0.005 psu. The freshening of the sea surface is typical of saline circulation induced by sinking within a region of strong evaporation. Notice that the oscillation is baroclinic in nature, so the barotropic structure is steady. In fact, the barotropic streamfunction reaches to the equilibrium state about one year after spinup from a state of rest. The freshwater flux drives a barotropic circulation, the so-called Goldsbrough–Stommel gyres (Fig. 6a). There is an anticyclonic gyre in the northern basin, driven by the precipitation, with a maximum mass flux of about 0.7 Sv, and a cyclonic gyre in the southern basin driven by the evaporation. The boundary between these two gyres is located at 37°N, which is very close to the $\phi_0 = 38.9$°N boundary based on the inviscid theory. Since the Coriolis parameter approaches zero at the equator, the strength of the cyclonic gyre is much weaker than that of the anticyclonic gyre to the north.

As discussed in the previous section, the barotropic velocity is divided into two parts. The first part is described in terms of the barotropic streamfunction that is shown in Fig. 6a. The second part is represented in terms of the barotropic potential function. The vertically integrated mass flux through each box is the sum of these two parts (Fig. 6b). In the subpolar basin interior both of these two components are southward, resulting in somewhat stronger southward mass flux in the subpolar basin. The total southward mass flux in the oceanic interior is about 0.7 Sv, which is smaller than the results based on the inviscid Goldsbrough relation shown in Fig. 4. These two components have different signs in the subtropic basin, so the sum of these two parts is a weak poleward flow in the interior. Therefore, the barotropic velocity (mass flux) due to evaporation and precipitation is very weak (about a few percent of that due to wind-driven circulation); however, as will be shown shortly, this tiny freshwater flux can drive a very strong three-dimensional circulation in the basin.

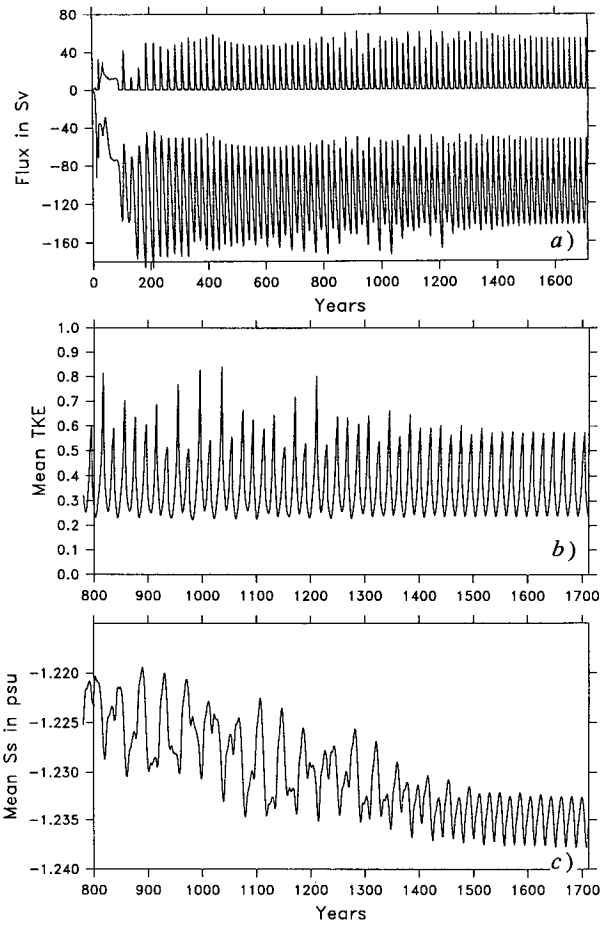

FIG. 5. Spinup of the model from the initial state of a homogeneous ocean. (a) Mass fluxes of the direct (low curve) and the indirect (upper curve) meridional cells (in Sv); (b) mean kinetic energy (in erg cm^{-3}); and (c) mean surface salinity (deviation from 35 psu).

Near the western wall there are western boundary currents whose existence is required for closing the mass flux, as discussed by Stommel (1957). Notice that the western boundary current is quite broad, and this is due to the low resolution used in this study.

The idea that precipitation and evaporation can drive large-scale circulation was proposed by Goldsbrough (1933). What Goldsbrough sought were the barotropic gyres driven by the vertical velocity imposed

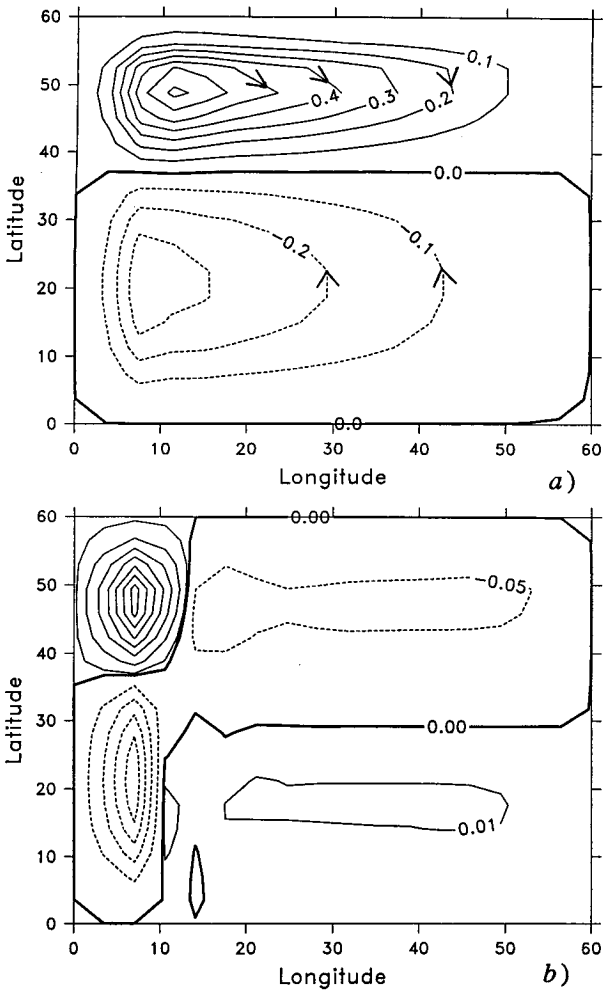

FIG. 6. (a) Barotropic streamfunction and (b) integrated meridional mass flux through each box (in Sv).

on the upper surface by precipitation and evaporation. If there was no salt in the oceans, the freshwater flux-driven circulation would have the simple barotropic structure discussed by Goldsbrough (1933) and Stommel (1957). However, there is salt in the oceans, and mixing of fresh water with saline water can produce a very strong baroclinic circulation in the basin. Nevertheless, many important aspects of the saline circulation driven by freshwater flux have been ignored so far. In the remaining part of this study I will concentrate on the time-mean, averaged over one period, three-dimensional structure of the saline circulation induced by mixing. The salt oscillation, its spatial structure, time evolution, and physical mechanism will be discussed in separate papers.

Judging by the magnitude, the amount of fresh water going through the system is tiny, just about 0.3 Sv. It seems negligible compared with the barotropic mass flux driven by the wind stress. It is probably the reason why it has been overlooked for so long. However, in the absence of the thermal forcing this tiny amount of fresh water alone can drive a huge baroclinic circulation in a three-dimensional basin. First, by integrating zonally, one obtains a strong meridional cell, with strong sinking at the equator and upwelling elsewhere. The maximum mass flux of this meridional cell reaches 108.6 Sv (Fig. 7a). This meridional cell is directly driven by the meridional pressure gradient induced by the meridional salinity gradient, as seen in Fig. 7c. That a small amount of fresh water (0.3 Sv) can drive a large circulation of 108.6 Sv implies an amplification factor of 350. Given such amplification, the model's response to the forcing must be very sensitive, so any small change in the forcing and in the model formulation may give rise to noticeable changes in the model's behavior.

The strength of the meridional overturning, 108.6 Sv, seems too large. Since mixing is the primary driving force for the circulation, the strength of the meridional cell could be reduced if small vertical mixing coefficients are used in the numerical experiments. The results of a parameter study of the model will be published in another paper (Huang and Chou 1993). In addition, the thermohaline overturning cell in the oceans is determined by the combined effects of heat and freshwater flux, which work against each other. As a result, meridional overturning cells in the oceans are much weaker.

Integrated meridionally, one can calculate the zonal streamfunction (Fig. 7b). There are three zonal cells. Within the top few hundred meters there is an anticyclonic cell characterized by sinking along the western boundary, the total mass flux of this cell is slightly more than 5 Sv. The major feature is a direct cell with sinking near the eastern boundary and upwelling in the interior, whose strength is about 30 Sv. This clockwise cell is driven by the east–west salinity gradient, as seen in Fig. 7d. In the abyss and off the eastern boundary there is an indirect cell, whose maximum mass flux is 10 Sv.

The salinity distribution is characterized by the relatively fresh water in the upper ocean and the relatively salty water in the deep ocean. There is a prominent halocline in the upper ocean, as seen in Figs. 7c,d.

Looking from above, one would see two horizontal gyres rotating in opposite directions. In the upper ocean, from level 1 to level 7 (760 m deep), there is an anticyclonic surface gyre and a cyclonic deep gyre below. By integrating the meridional velocity one can obtain a baroclinic streamfunction map. The maximum mass flux of the surface gyre is about 15 Sv, as shown in Fig. 8. (Notice that, in the horizontal plane, the motion is not without divergence, so the velocity field should be described as the sum of the contribution from a streamfunction and a potential function.) There is clearly an anticyclonic gyre in the northern part of the basin. In the southern basin, the velocity is domi-

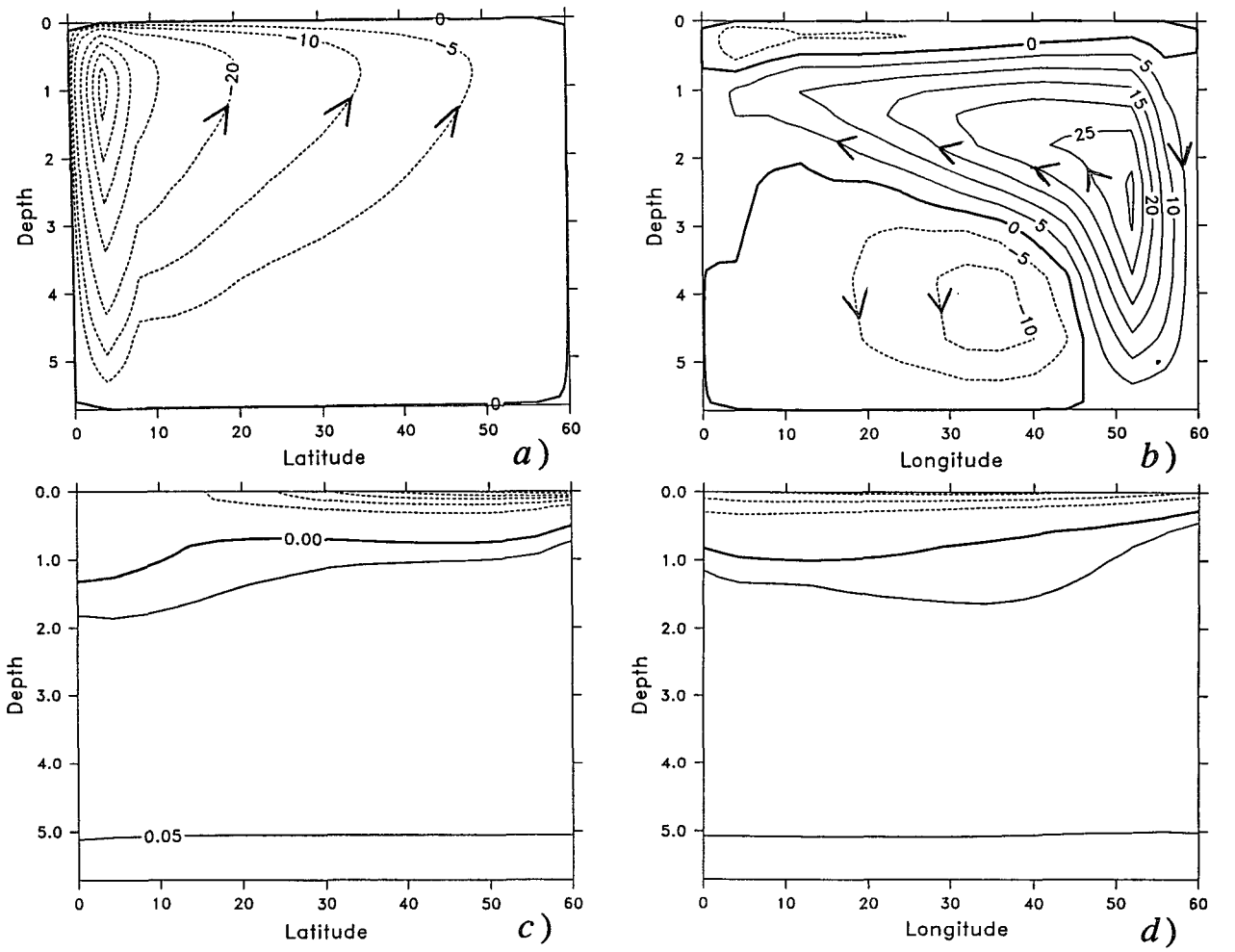

FIG. 7. Time-mean circulation patterns, depth in kilometers. (a) Meridional streamfunction in Sverdrups. Notice that contour interval is 20 Sv for the unlabeled curves. (b) Longitudinal streamfunction. (c) Zonally mean meridional salinity distribution (deviation from the mean salinity). (d) Meridionally mean zonal salinity distribution (deviation from the mean salinity), both in practical salinity units. Interval is 0.05 psu for the solid contours and 0.5 psu for the dashed contours.

nated by sinking motion; thus, the streamfunction alone does not give a complete circulation pattern.

The upper-layer velocity field is characterized by a well-defined anticyclonic gyre, Fig. 9. Along the southern boundary the strong velocity component perpendicular to the wall implies strong sinking along the equator. There is also sinking along the western boundary, indicated by the velocity convergence near the western wall. Along the northern boundary the Goldsbrough relation requires a nonzero meridional velocity; thus there is a frictional northern boundary current to satisfy the no-flow condition, as shown by the eastward current near the northern boundary in Fig. 9. At deeper levels the center of the anticyclonic gyre moves westward and its strength declines.

The sea surface salinity distribution, Fig. 10a, shows a prominent north–south and east–west gradient. A layer of relatively fresh water covers most of the upper surface except the southeastern corner. The freshening

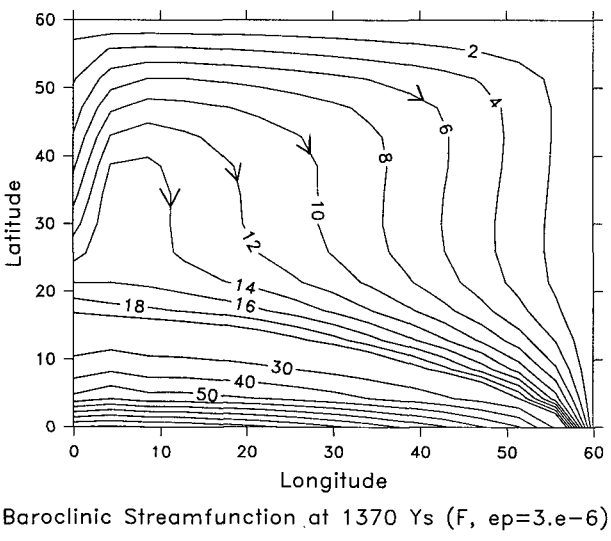

FIG. 8. Horizontal baroclinic streamfunction (in Sv).

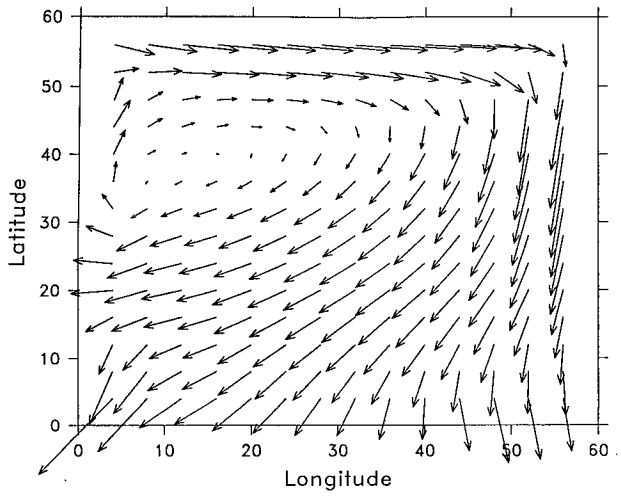

FIG. 9. Horizontal velocity vector diagram at the upper surface.

of the surface water is the major feature of a saline circulation. Within the upper ocean the flow is close to geostrophic except near the western boundary. That salinity is higher at the eastern/western boundaries than that at the interior is consistent with the geostrophic constraint. Accordingly, the surface salinity reaches its maximum at the southeastern corner, and this is the region where bottom water in the model is formed. As a result, although sinking takes place along the entire southern boundary, bottom water is formed only at the southeastern corner. At a depth of 302 m, the horizontal salinity contours resemble the anticyclonic gyre very closely. Notice that the meridional salinity gradient reverses sign near the northern boundary at depth 302 and 643 m. This reverse of meridional salinity gradient gives rise to a southward salt flux due to diffusion, as will be shown shortly. The depth map of the halocline, defined as the zero salinity interface, also serves as a good indicator of the anticyclonic gyre in the upper ocean, as shown in Fig. 11.

For comparison, a test run of an old model based on the virtual salt flux has been carried out. One of the difficulties in using the virtual salt flux formulation is that the mean surface salinity is unknown before the solution is found. Here, we have used the basin-mean salinity $\bar{S} = 35$ psu. All other parameters are identical with those in case 1 except the vertical velocity is set to zero at the upper surface. The model is spun up from the same initial state of rest, with the basin-mean salinity equal to 35 psu. The spinup processes for these two models are slightly different, as shown in Fig. 12. The main difference is that the old model gives rise to relatively fresher water in the subpolar basin. Notice that the virtual salt flux is exact at the beginning of the spinup. However, as the halocline is gradually developed, the mean surface salinity drifts toward a lower value. As a result, the virtual salt flux formulation tends to exaggerate the salt flux, especially in the subpolar basin because the local salinity is the lowest.

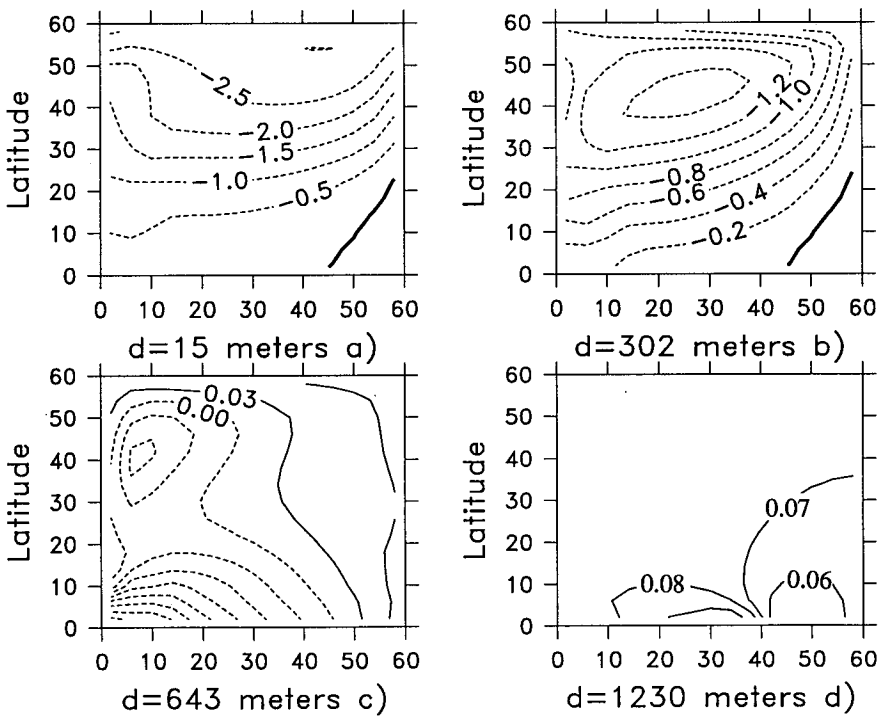

FIG. 10. Salinity (deviation from 35 psu) distribution at 15, 302, 643, and 1230 m (in psu).

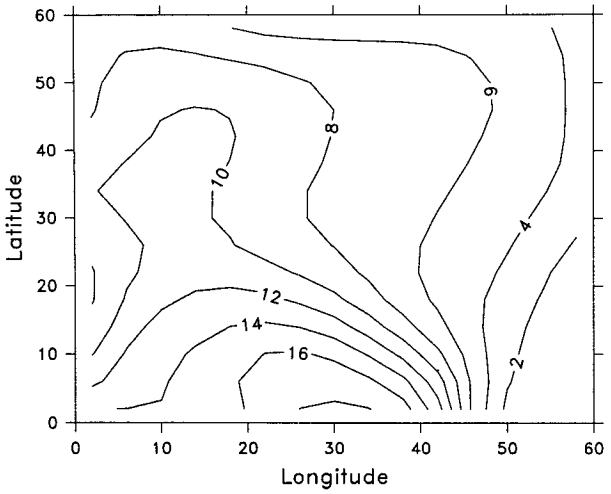

FIG. 11. Depth of the halocline (zero salinity perturbation surface), in 100 m.

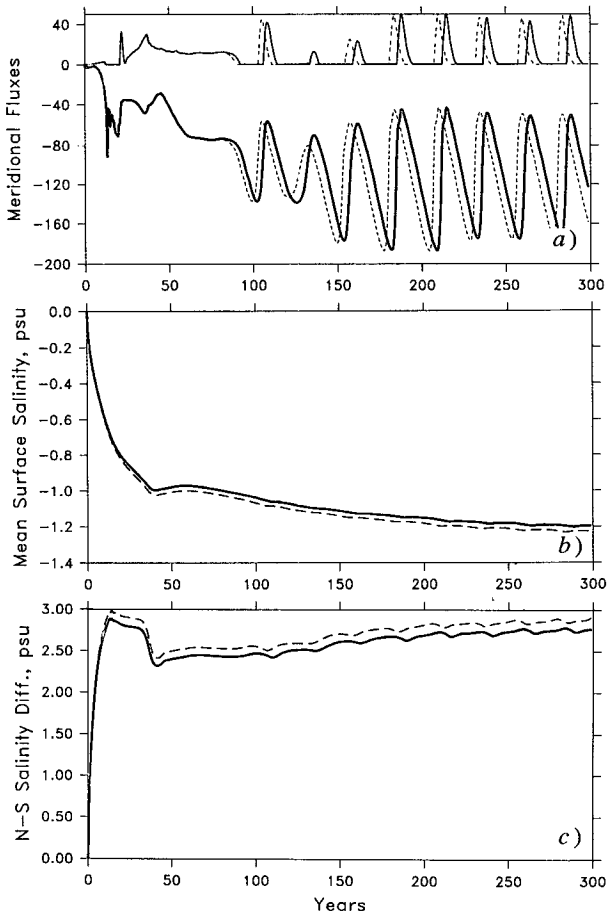

FIG. 12. Comparison of spinup process for the new model (solid lines) and the old model based on virtual salt flux (dashed lines); (a) the strength of meridional overturning cells (in Sv); (b) mean surface salinity (deviation from 35 psu); (c) mean north–south salinity difference (in psu).

After 1712 years, the model reached a state of oscillation with a period of 40.48 years (slightly more than doubling the 18.87-year period of the new model). Given the period doubling, the oscillation characteristics are quite different from case 1. For example, the mean kinetic energy has much higher spikes, as shown in Fig. 13, compared with case 1. However, the time-mean solution of the old model is rather similar to the new model, with a difference of a few percent for most quantities. For example, the strength of the direct meridional overturning cell is −108.6 Sv for the new model and −112.7 Sv for the old model; the mean surface salinity (deviation from 35 psu) is −1.235 psu for the new model and −1.254 psu for the old model; the north–south surface salinity difference (defined as the mean surface salinity of the southernmost row of grid boxes minus that of the northernmost row) is 2.840 psu for the new model and 2.961 psu for the old model.

The most important difference between these two formulations is the surface salinity. As shown in Fig. 14, the time-mean surface salinity in the interior ocean for the old model is lower than the new model. The largest difference reaches 0.125 psu in the subpolar basin. Near the western boundary the salinity in the old model is higher than the new model, with a maximum value of 0.183 psu around 16°N. Although the differences between these two models seem minor, it may be critical for the thermohaline circulation. In fact, a 0.125 psu difference in salinity can be decisive in determining whether the cold surface water formed in the subpolar basin would sink or not. One of the cases of most concern is whether the deep-water formation

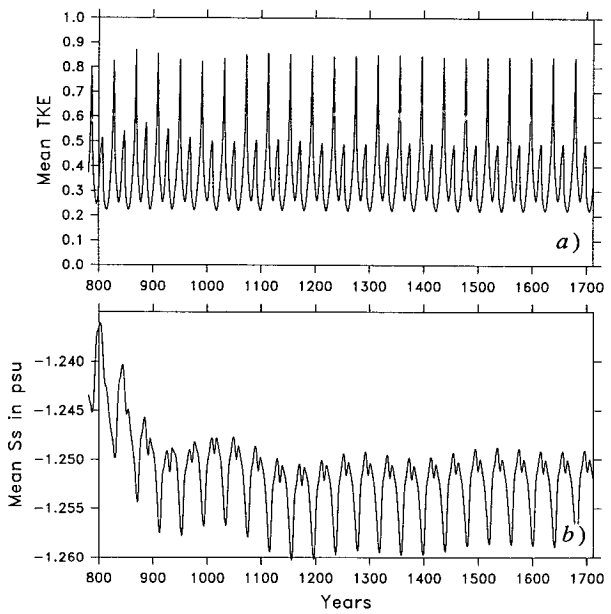

FIG. 13. Time evolution of an old model based on virtual salt flux. (a) Mean kinetic energy (in erg cm^{-3}); (b) mean surface salinity (deviation from 35 psu).

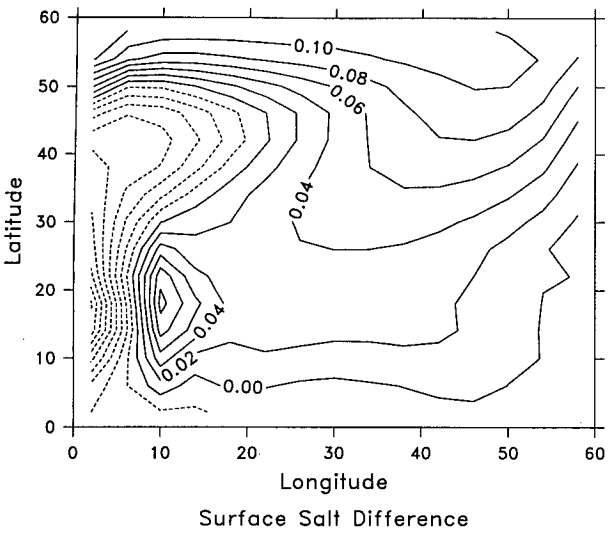

FIG. 14. Difference in surface salinity, the new model minus the old model (in psu).

in the North Atlantic will be interrupted due to changes in atmospheric forcing, such as air–sea heat flux and freshwater flux. The thermohaline circulation in the North Atlantic is believed to be close to a critical state, so small perturbations may trigger a "haline catastrophe." In regard to the potential importance of accurate understanding of the thermohaline circulation, it seems important to simulate the salinity balance as accurately as possible.

The major advantage of the new model is the correct simulation of the meridional salt flux. It was previously noticed that the meridional salt flux calculated from models based on virtual salt flux was an artifact. In his pioneering work, Bryan (1969b) pointed out that the meridional salt flux should be interpreted as a meridional freshwater flux in the opposite direction. Semtner and Chervin (1992) have carried out a very ambitious simulation of the global oceanic circulation; they have also calculated the meridional salt fluxes due to advection and eddies. So far, however, the dynamic meaning of the meridional salt fluxes has remained obscure.

With the new model, the meridional freshwater and salt fluxes are simulated much more accurately. As the model is spun up from an initial state of homogeneous ocean, there is a large southward salt flux due to the equatorward motion of fresh water from precipitation in the subpolar basin, which drives the barotropic circulation in the model. As the meridional overturning cell develops, the meridional salt flux due to the baroclinic circulation increases. It is readily seen that the meridional salt flux due to the baroclinic cell is opposite to the salt flux due to the barotropic velocity.

In fact, the meridional salt flux consists of two terms:

$$F^S = F^S_{ad} + F^S_{df},$$

where $F^S_{ad} = \int\int vS dxdz$ is the salt flux due to advection, and

$$F^S_{df} = -\int\int k_s \frac{\partial S}{\partial y} dxdz$$

is the salt flux due to diffusion, which is a parameterization for the eddies. The advective salt flux can be divided into three parts by noting that $v = \bar{v} + v'$, where $\bar{v}$ is the barotropic velocity and v' is the baroclinic velocity, and $S = \bar{S} + S'$, where $\bar{S} = 35$ psu is the basin-mean salinity. Therefore, one obtains

$$\int\int vS dxdz = \bar{S}\int\int v dxdz + \int\int v'S' dxdz + \bar{v}\int\int S' dxdz.$$

The first term on the right-hand side is the contribution due to barotropic velocity. Because of the excess precipitation in the subpolar basin, this term is always negative and it is the dominant term in the beginning of the spinup process. The second term is due to the baroclinic velocity. Because in a saline circulation both v' and S' are negative in the upper ocean and positive in the deep ocean, this term is positive. Notice that this term remains positive in a thermal mode of circulation, in which both v' and S' are positive in the upper ocean and negative in the deep ocean. The third term is small because S' changes sign with depth, and the sign of this term is unclear. Therefore, the advective salt flux is primarily controlled by the contributions from the first and second terms. The major deficit of the old model is the lack of the barotropic term, although this is implicitly remedied by introducing the virtual salt flux at the upper surface. Nevertheless, such a virtual flux can be conceptually misleading.

As the model reaches a quasi equilibrium, the advective salt flux due to the baroclinic cell almost counterbalances that due to the barotropic gyres. The net advective salt flux is roughly balanced by the diffusive salt flux, as shown in Fig. 15a for a section at 28°N. In comparison, the meridional salt flux in the old model is covered up by the artifact of the model. As shown in Fig. 15b, the advective salt flux is zero in the beginning of the spinup process because the velocity is very small at this stage. When the model is spunup, the meridional salt flux due to advection is large. That both advective and diffusive salt flux are poleward at 28°N is really an artifact of the old model; the sum of the two is the meridional virtual salt flux. Although it has been argued in previous studies that the meridional salt flux should be interpreted as the freshwater flux in the opposite direction, it is not clear how to interpret different components of the meridional salt flux. For example, one can ask whether meridional salt flux due to eddies contributes to freshwater flux or not. According to the results from the new model, one can interpret the salt fluxes from the old model by subtracting a meridional salt flux due to freshwater flux,

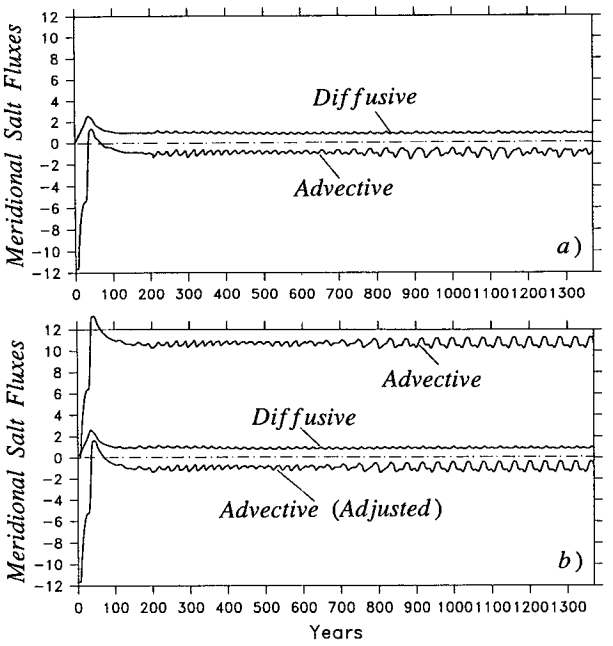

FIG. 15. Time evolution of the meridional salt fluxes at 28°N, in 10^6 kg s^{-1}: (a) the new model; (b) the old model based on virtual salt flux.

which is absent in the old model. With this adjustment, the meridional salt fluxes of the old model look similar to the new model, and the time-mean (adjusted) advective meridional salt flux is balanced by that due to diffusion.

As the models reach the final state of regular oscillation after 1600 years, the meridional advective salt flux also oscillates in phase with the diffusive salt flux. As a result, the total meridional salt flux oscillates with the same period, shown in Fig. 16. From the results of the model, it is speculated that in the real oceans the meridional salt flux due to eddy diffusion and advection are nonzero, and they may also oscillate due to the variabilities of the circulation.

The horizontal distribution of the meridional salt fluxes is shown in Fig. 17. The advective and diffusive salt fluxes in the new model are shown in the left part of the figure. Notice that the advective salt flux is dominated by the barotropic Goldsbrough–Stommel flow. For example, the strong salt flux near the western boundary, Fig. 17a, is due to the strong western boundary currents, as predicted by Stommel. As a result, there is a poleward advective salt flux at high latitudes. In comparison, the advective salt flux for the old model, shown in Fig. 17b, is dominated by poleward flux in the ocean interior and equatorward flux near the western boundary, which are primarily due to the anticyclonic surface gyre. It is important to notice that the advective salt flux in the old model lacks the barotropic component, which is dominant in Fig. 17a. The salt flux due to diffusion is very similar for both models. Notice that the diffusive salt flux is equatorward near the northern boundary, which is due to the reverse meridional gradient of salinity at middepth, as shown in Figs. 10b and 10c.

The foregoing discussion has been concentrated on one section at 28°N; the time-mean meridional salt fluxes at other sections are depicted in Fig. 18. Since the advective salt flux due to the barotropic velocity is always equatorward and that due to the baroclinic velocity is always poleward, the sign of the meridional advective salt flux depends on the competition between these two components. Apparently, the barotropic salt flux is dominant south of 46°N, but the baroclinic salt flux is dominant in the northern basin. Because the sum of all salt fluxes should be zero, the salt flux due to diffusion has the exact value of that due to advection but with a different sign.

It is important to notice that even if the circulation reaches a steady state, the total meridional salt flux in the world oceans is nonzero. The existence of meridional salt flux is due to the interbasin freshwater transport. For example, the water flux through the Bering Strait is about 0.8 Sv. This leads to a meridional salt flux that must be constant in the North Pacific and North Atlantic basins. According to the estimation made by Wijffels et al. (1992), the total meridional salt flux in the Atlantic is -26.7×10^6 kg s^{-1} (southward), which is about 30 times stronger than the advective salt flux calculated for the time-mean circulation in the present model. It is important to notice that

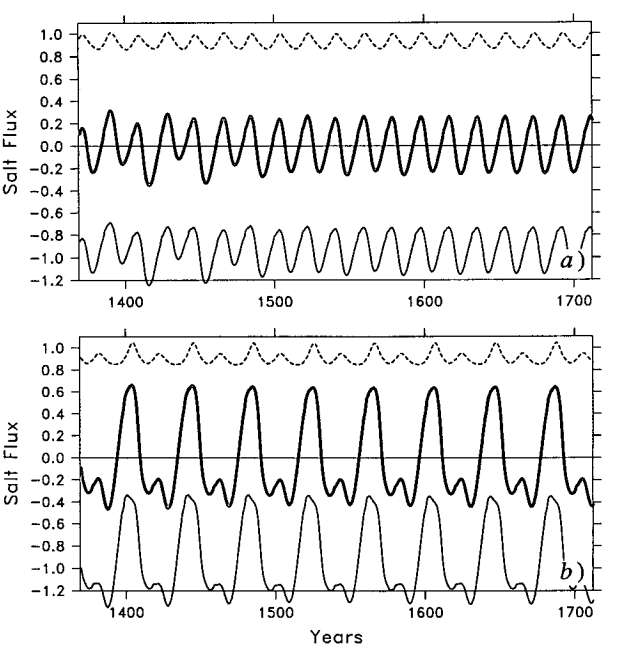

FIG. 16. Meridional salt fluxes, in 10^6 kg s^{-1}. (a) The new model: the thin solid line indicates the advective salt flux, the dashed line the diffusive salt flux, and the heavy solid line the total salt flux. (b) The old model: the thin solid line indicates the adjusted advective salt flux, the dashed line the diffusive salt flux, and the heavy line depicts the sum of the two salt fluxes. Notice that the salt oscillation in these two models has quite different characteristics.

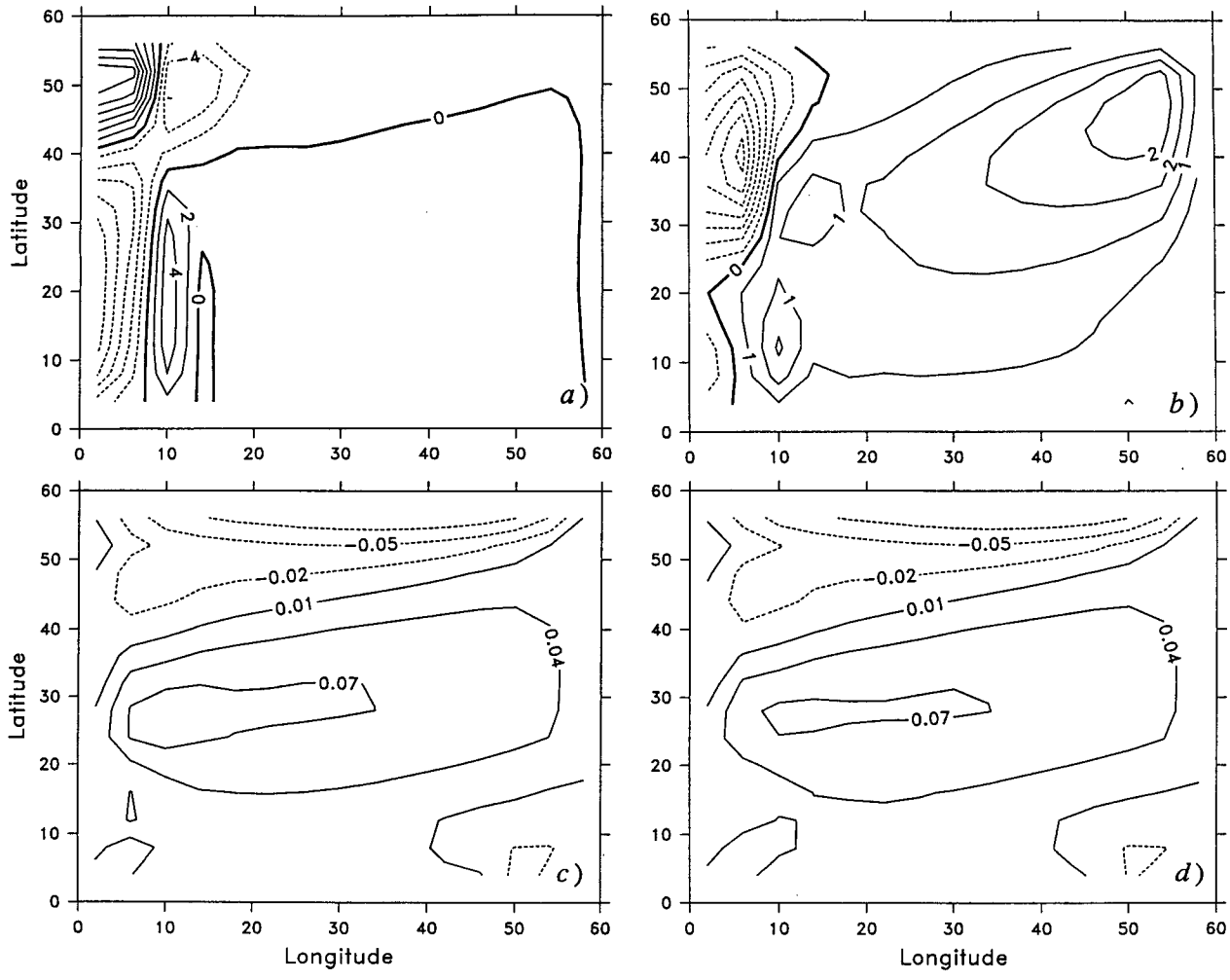

FIG. 17. Horizontal maps of poleward salt fluxes, in 10^6 kg s^{-1} per 4° longitude: (a) advective salt flux for the new model, (b) advective salt flux for the old model, (c) diffusive salt flux for the new model, and (d) diffusive salt flux for the old model.

the meridional advective salt flux need not be constant in each basin. As previously discussed, the contribution due to eddies varies with latitude, so the meridional advective and eddy salt fluxes are not constant.

5. Conclusions

The relaxation condition and the so-called mixed boundary conditions are inappropriate for ocean forecasting and climate modeling. First, both these boundary conditions imply a nonphysical virtual salt flux across the air–sea interface and through the ocean and atmosphere. Second, these two conditions can introduce systematic errors. A natural way of formulating the upper boundary condition for the salinity balance in primitive models has been proposed and tested in the simplest situations of a purely freshwater-forced system. Formulated on the base of real physics, the natural boundary conditions are more accurate and easy to apply. Although the discussion in this study has been focused on a model without a mixed layer on the top, it seems rather straightforward to apply the natural boundary condition to the case including a mixed layer on the top. One can hardly exaggerate the importance of using the natural boundary conditions for oceanic models. It is suggested that the natural boundary condition could be used for all models in-

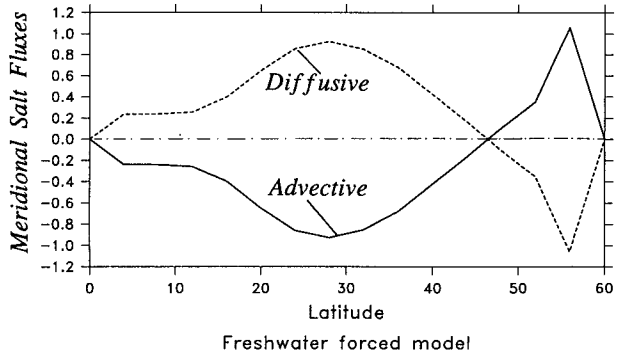

FIG. 18. Meridional profile of poleward salt fluxes, in 10^6 kg s^{-1}.

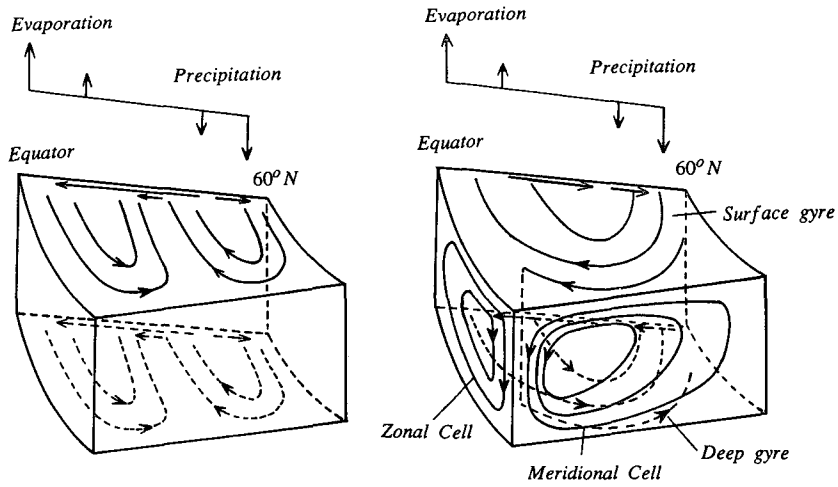

a) The Barotropic Goldsbrough–Stommel gyres. *b) The Baroclinic Structure.*

FIG. 19. Schematic structure of the saline circulation driven by precipitation at high latitude and evaporation at low latitude.

volving a salinity balance, such as mixed-layer models, ice–ocean coupling models, and atmosphere–ocean coupling models.

The numerical experiments for the case of an idealized freshwater-forcing model reveal the very interesting structure of the saline circulation driven solely by precipitation and evaporation. First, the Goldsbrough–Stommel gyres have been reproduced. Second, the model's results reveal the intricate three-dimensional structure of the saline circulation implied by the barotropic Goldsbrough–Stommel gyres. In fact, there are very strong circulations in the meridional, zonal, and horizontal planes. The strength of these circulations is two orders of magnitude larger than the forcing itself. Given such big amplification factors, it is easy to understand that the model is very sensitive to any changes in the forcings and the parameters. Third, the model reproduces salt oscillation forced by freshwater flux alone. It seems very important to study such oscillations more carefully in order to understand the salt oscillation in the general case with more complicated forcings.

The most important results of this study can be summed up in Fig. 19. On the left are the barotropic Goldsbrough–Stommel gyres driven by evaporation minus precipitation. There is an anticyclonic gyre in the subpolar basin and a cyclonic gyre in the subtropic basin, including western boundary currents required for closing the circulation. These barotropic gyres are very weak, with a maximum volume flux of no more than 1 Sv. However, such a weak plain water flux induces a very strong baroclinic circulation in the basin, shown in Fig. 19b. There is a very strong meridional overturning cell and a zonal overturning cell, which is a hundred times stronger than the barotropic circulation. In the vertical direction, there is a surface gyre within the top kilometer and a deep gyre below, which has a mass flux of about 15 Sv. Notice that the western boundary current of the surface gyre flows northward. Since the surface gyre is a hundred times stronger than the barotropic Goldsbrough–Stommel gyres, the baroclinic structure dominates the structure.

Although it seems clear (theoretically) that the meridional salt flux and freshwater flux are extremely important components of the thermohaline circulation, these fluxes have never been exactly simulated in oceanic general circulation models and their dynamic roles have been obscure. The results from the new model provide some insight into the dynamical roles of the meridional salt fluxes. The balance between the advective salt fluxes due to barotropic and baroclinic circulation and the diffusive salt flux is of most importance. It is expected that as the model becomes more elaborate and the forcing becomes more complex, the evolution of the meridional salt flux will be more intricate. It is hoped that the result from the new model will stimulate interest in this issue.

The results presented in this study are among many experiments carried out so far. Since the appropriate handling of salinity in ocean models has been overlooked for so long, there are many urgent numerical tests to be carried out. The general cases combining freshwater forcing with thermal forcing and wind stress are under way currently and will be published later.

Acknowledgments. I have benefited from conversations with my most respected friend Henry Stommel. Hank, with his deep physical insight and his enthusiasm about Goldsbrough gyres, was a continuous source of inspiration. Ru Ling Chou helped to set up the numerical model used in this study. It is a pleasure to acknowledge helpful conversations with my colleagues Kirk Bryan, Jim Luyten, Joe Pedlosky, and Ray

Schmitt. Constructive comments from reviewers have been very helpful in improving the text. This study was supported by the National Science Foundation through Grant OCE 90-17158 and Office of Naval Research Grant N00014-90-1518. Part of the calculations were carried out on the CRAY-YMP at the National Center of Atmospheric Research at Boulder, Colorado, which is supported by the National Science Foundation.

APPENDIX

The Rigid-Lid Approximation

The physical boundary condition on the free surface is

$$w = \frac{D\eta}{Dt} + e, \quad \text{at} \quad z = \eta, \tag{A1}$$

where w is the vertical velocity,

$$\frac{D}{Dt} = \frac{\partial}{\partial t} + u\frac{\partial}{\partial x} + v\frac{\partial}{\partial y}$$

is the total derivative, η is the free surface elevation, and $e = E - P$ is the evaporation minus precipitation. For the motions in the ocean interior, the following scaling can be used

$$(x, y) = L(x', y') \quad (u, v) = U(u', v') \tag{A2}$$

$$t = Tt', \quad \eta = \frac{fLU}{g}\eta' \tag{A3}$$

$$w = \delta U w', \quad e = \lambda\delta U e', \tag{A4}$$

where $\delta = H/L \ll 1$ is the aspect ratio, and $\lambda \approx 0.01 \ll 1$. An assumption has been made that the time scale is determined by the horizontal advection. Substituting these relations into the boundary condition and dropping the primes, one obtains

$$w = \varepsilon_T F\frac{\partial\eta}{\partial t} + \varepsilon F\mathbf{u}\cdot\nabla\eta + \lambda e, \quad \text{at} \quad z = \varepsilon F\eta, \tag{A5}$$

where $\varepsilon_T = 1/fT \ll 1$ is the Kible number, $\varepsilon = U/fL \ll 1$ is the Rossby number, and

$$F = \frac{f^2L^2}{gH} = \left(\frac{L}{R}\right)^2 \approx O(1),$$

where $R = \sqrt{gH}/f$ is the deformation radius. If the advection time scale L/U is chosen as the time scale, the first two terms are of the same magnitude. For motions with horizontal scale of 1000 km, the nondimensional number εF is about 10^{-4}, which is much smaller than λ. Thus, the upper boundary condition can be linearized as

$$w = e \quad \text{at} \quad z = 0. \tag{A6}$$

The rigid-lid approximation is not accurate for motions with time scale shorter than decadal, motions on the planetary scale, or motions in the shallow seas. For example, for motions of planetary scale, $L = 10^9$ cm, for wave motion on seasonal time scales or shorter, $T \leqslant 10^7$ s, so $\varepsilon_T F \approx 0.02$. Thus, the vertical velocity due to wave motions of the free surface elevation has the same magnitude as that of the evaporation minus precipitation. Under such circumstances, the rigid-lid approximation, in which the free surface motion is neglected, is inaccurate. Since the focus of this study is on the large-scale circulation on climate time scale, the rigid-lid approximation is valid.

REFERENCES

Baumgartner, A., and E. Reichel, 1975: *The World Water Balance.* Elsevier, 179 pp.

Broecker, W. S., D. M. Peteet, and D. Rind, 1985: Does the ocean–atmosphere system have more than one stable mode of operation? *Nature,* **315,** 21–26.

Bryan, F., 1986: High-latitude salinity effects and interhemispheric thermohaline circulations. *Nature,* **323,** 301–304.

Bryan, K., 1969a: A numerical method for the study of the circulation of the world ocean. *J. Comput. Phys.,* **4,** 347–376.

——, 1969b: Climate and the ocean circulation. III: The ocean model. *Mon. Wea. Rev.,* **97,** 806–827.

Goldsbrough, G. R., 1933: Ocean currents produced by evaporation and precipitation. *Proc. Roy. Soc. London,* **A141,** 512–517.

Haney, R. L., 1971: Surface thermal boundary condition for ocean circulation models. *J. Phys. Oceanogr.,* **1,** 241–248.

Hough, S. S., 1897: On the application of harmonic analysis to the dynamical theory of the tides. Part I: on Laplace's "Oscillations of the first species," and on the dynamics of ocean currents. *Philos. Trans.,* **A189,** 201–258.

Huang, R. X., and R. L. Chou, 1993. A parameter study of the saline circulation. *Climate Dyn.,* in press.

——, and R. W. Schmitt, 1993. The Goldsbrough–Stommel circulation of the world oceans. *J. Phys. Oceanogr.,* **23,** 1277–1284.

——, J. R. Luyten, and H. M. Stommel, 1992. Multiple equilibrium states in combined thermal and saline circulation. *J. Phys. Oceanogr.,* **22,** 231–246.

Killworth, P. D., 1989. On the parameterization of the deep convection in ocean models. *Parameterization of Small-Scale Processes.* P. Muller and D. Henderson, Eds., Hawaii Institute of Geophysics Special Publication, 59–74.

——, D. Stainforth, D. J. Webb, and S. M. Paterson, 1991: The development of a free-surface Bryan–Cox–Semtner ocean model. *J. Phys. Oceanogr.,* **21,** 1333–1348.

Niiler, P. P., and E. B. Kraus, 1977. *One-Dimensional Models of the Upper Ocean.* E. B. Kraus, Ed., Pergamon, 143–172.

Rooth, C., 1982: Hydrology and ocean circulation. *Progress in Oceanography,* Vol. 11, Pergamon, 131–149.

Schmitt, R. W., P. S. Bogden, and C. E. Dorman, 1989: Evaporation minus precipitation and density fluxes for the North Atlantic. *J. Phys. Oceanogr.,* **19,** 1208–1221.

Semtner, A. J., Jr., and R. M. Chervin, 1992: Oceanic general circulation from a global eddy-resolving model, *J. Geophys. Res.,* **97**(C4), 5493–5550.

Stommel, H. M., 1957: A survey of ocean current theory. *Deep-Sea Res.,* **4,** 149–184.

——, 1961: Thermohaline convection with two stable regions of flow. *Tellus,* **13,** 224–230.

——, 1984: The delicate interplay between wind-stress and buoyancy input in ocean circulation: The Goldsbrough variations. *Tellus,* **36A,** 111–119.

Wijffels, S. E., R. W. Schmitt, and H. L. Bryden, 1992: Transport of freshwater by the oceans. *J. Phys. Oceanogr.,* **22,** 155–162.